

## Mixing of bound states with electron transport by a radiation field in waveguides

E. N. Bulgakov

*Kirensky Institute of Physics, Siberian Branch of Russian Academie of Sciences, 660036 Krasnoyarsk, Russia*

A. F. Sadreev\*)

*Kirensky Institute of Physics, Siberian Branch of Russian Academie of Sciences, 660036 Krasnoyarsk, Russia; Abo Akademi, Institutionen för Fysik, Department of Physics SF-20500, Abo, Finland*  
(Submitted 3 March 1998)

Zh. Éksp. Teor. Fiz. **114**, 1954–1970 (December 1998)

Electron transmission in the two-, three-, and four-terminal nanostructures is considered under the influence of a radiation field. The frequency of the radiation field is tuned to the transition between the energy of a bound state and the Fermi energy of the incident electrons. The radiation induced resonant peaks and dips of the electron transport are exhibited for zero and low magnetic fields. It is shown that rotation of the radiation field polarization can effectively control the electron transport into different electrodes attached to the structures because of the symmetry of the structures. The resonant anomalies of the Hall resistance are found in a weak magnetic field. © 1998 American Institute of Physics. [S1063-7761(98)00412-0]

### 1. INTRODUCTION

For several decades the transport of electrons in structures of low dimensionality and complicated geometry has been the focus of extensive theoretical and experimental study. Electrons can be confined to very narrow regions fabricated on an interface of an AlGaAs/GaAs heterostructure. Since the electrons in such regions can have high mobilities in the two dimensions available to them, such systems are called two-dimensional electron gases (2DEGs). The study of electronic transport properties of 2DEGs is of great current interest not only from the standpoint of the basic quantum effects involved but also for potential engineering applications. An idealized sample becomes an electron waveguide, wherein the quantum transport properties are solely determined by the geometry of the structure and the wavelike nature of the electrons. A remarkable manifestation of the successful achievement of quantum ballistic transport through a semiconductor nanostructure is the appearance of quantized steps on the conductance through a narrow structure as the number of one-dimensional channels is successively varied,<sup>1,2</sup> the quenching of the Hall effect, and the last plateau and the negative bend resistance in the cross geometry.<sup>3–5</sup>

Ford *et al.*<sup>5</sup> presented a systematic investigation of the influence of cross geometry on the Hall effect. They fabricated various differently shaped cross sections based on GaAs–Al<sub>x</sub>Ga<sub>1–x</sub>As, which demonstrated that near zero magnetic field the Hall resistance can be quenched, enhanced over its classical value, or even negative. This effect has been considered in detail theoretically by Schult *et al.*<sup>6</sup> and Amemiya and Kawamura.<sup>7</sup> Another interesting feature of the cross geometries is a bound state found numerically by Schult *et al.*<sup>8</sup> and by Peeters.<sup>9</sup>

The question of the existence of electromagnetic modes trapped by special geometries has been a classic one in the

theory of waveguides.<sup>10</sup> It has been realized that the introduction of bends into waveguides generally leads to bound states, or localized modes, which exist below the cut-off frequency for the waveguide. Carini *et al.*<sup>11,12</sup> have demonstrated theoretically and experimentally the presence of bound *TE* modes for rectangular bent waveguides and shown that the number of bound *TE* modes is bend-dependent. For the two-dimensional Schrödinger equation it was proved that any curved two-dimensional waveguide of constant width and infinite length posses bound states.<sup>13–18</sup> Bound states were found in the same year (1989) in a four-terminal junction of narrow wires by Schult<sup>6,8</sup> and independently by Peeters<sup>9</sup> (see also Refs. 19 and 20).

For the stationary processes of the energy conserved electron transmission only quasi-bound states with energies within the conduction subbands are important.<sup>6,7</sup> In particular, it was shown that the quasi-bound states in the Hall junction result in resonant dips of the resistance in high magnetic fields when the magnetic length is comparable with the size of the junction. The Hall resistance sensitively depends on the geometry of a junction and can become negative for a smoothed junction for small magnetic fields.

Although the bound states below the lowest subband threshold do not participate in stationary transmission, the possibility of observing of them, at least in principle, was shown by Berggren and Ji for the case of two intersecting electron waveguides with finite electrodes.<sup>20</sup> In that case bound states can be probed by resonant tunneling through the electrodes below the subband. However, it is possible to mix the bound state with electron transmission through electron waveguides with infinite electrodes directly by application of a radiation field, provided that the dipole matrix elements between the bound state and propagating ones are not equal to zero. Such a possibility was demonstrated for the four-terminal's Hall junction.<sup>21</sup> Let  $E_1$  be the energy of the bound

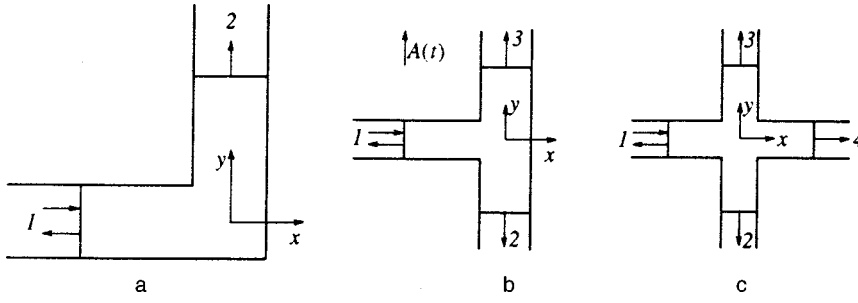


FIG. 1. The types of structures considered: *L*-structure (a), the *T*-structure (b), and *X*-structure (c).

state below the subbands which for zero magnetic field can be specified as

$$E_n(k) = \frac{\hbar^2}{2m^*d^2}(k^2 + \pi^2 n^2),$$

where  $d$  is the width of the electrodes,  $n$  is the number of the subband, and  $k$  is the wave number of the incident electron. Tuning a perturbation frequency near the resonance  $\hbar\omega = E_n(k) - E_0$ , one can expect resonant anomalies in the electron transmission through the many-terminal junctions.<sup>21</sup>

The aim of the present article is to consider the electron transmission effected by mixing of bound states with the propagating solutions in the *X*-, *T*-, and *L*-types of electron waveguides which are shown in Fig. 1.

## 2. CONDUCTANCE ANOMALIES INDUCED BY THE RADIATION FIELD

### 2.1. Numerical method

In this section we consider single electron transmission through the rectangular structures, the geometries of which are shown in Fig. 1 and specified below as *L*-, *T*-, and *X*-structures. They share the property of having at least one bound state. The Schrödinger equation for an electron of a mass  $m^*$  subjected to a magnetic field  $B$  applied normal to the junction and to a radiation field  $\mathbf{A}_1(t)$  directed in the plane of the junction can be written

$$i\hbar \frac{\partial \psi(\mathbf{r}, t)}{\partial t} = \frac{\hbar^2}{2m^*} \left( i\nabla + \frac{e}{\hbar c} (\mathbf{A}_0(\mathbf{r}) + \mathbf{A}_1 \cos \omega t) \right)^2 \psi(\mathbf{r}, t). \quad (1)$$

Here we use the gauge  $\mathbf{A}_0(\mathbf{r}) = (-By, 0, 0)$ . The radiation field is considered in the long-wavelength approximation, in which the wavelength of the radiation field is much greater than the size of the junction. We use the following dimensionless transformations:

$$t \rightarrow \frac{\hbar t}{2m^*d^2}, \quad \mathbf{r} \rightarrow \frac{\mathbf{r}}{d}, \quad \epsilon = \frac{2m^*d^2E}{\hbar^2},$$

$$\omega \rightarrow \frac{2m^*d^2\omega}{\hbar}, \quad \mathbf{a} = \frac{2\pi d\mathbf{A}_1}{\phi_0}, \quad \gamma = \frac{2\pi d^2B}{\phi_0}, \quad (2)$$

where  $\phi_0 = ch/e$  is the magnetic flux quantum. In terms of the dimensionless variables (2) the Schrödinger equation (1) takes the form

$$i \frac{\partial \psi(\mathbf{r}, t)}{\partial t} = (i\nabla + (\mathbf{a}_0(\mathbf{r}) + \mathbf{a} \cos \omega t))^2 \psi(\mathbf{r}, t), \quad (3)$$

where  $\mathbf{a}_0(\mathbf{r}) = (-\gamma y, 0, 0)$ . We map this equation onto a square lattice with elementary unit  $w$ . The lattice site is specified as  $(m, l)$ . The total vector potential  $\mathbf{a}_0 + \mathbf{a} \cos \omega t$  is accounted for by a Peierls phase factor.<sup>22</sup> Then Eq. (3) transforms as follows:

$$i w^2 \frac{\partial \psi(m, l)}{\partial t} = 4\psi(m, l) - \exp(i\tilde{\gamma}l)\psi(m+1, l) - \exp(-i\tilde{\gamma}l)\psi(m-1, l) - \exp(-i\tilde{a} \cos \omega t)\psi(m, l+1) - \exp(i\tilde{a} \cos \omega t)\psi(m, l-1), \quad (4)$$

where  $\tilde{\gamma} = \gamma w^2$ ,  $\tilde{a} = aw$ . In the four-terminal junction we use also a different gauge  $\mathbf{a}_0(\mathbf{r}) = (0, \gamma x, 0)$  for which the Schrödinger equation (3) will map onto a square lattice as follows:

$$i w^2 \frac{\partial \tilde{\psi}(m, l)}{\partial t} = 4\tilde{\psi}(m, l) - \tilde{\psi}(m+1, l) - \tilde{\psi}(m-1, l) - \exp(-i\tilde{a} \cos \omega t - i\tilde{\gamma}m)\tilde{\psi}(m, l+1) - \exp(i\tilde{a} \cos \omega t + i\tilde{\gamma}m)\tilde{\psi}(m, l-1), \quad (5)$$

where  $\psi(m, l) = \exp(-i\tilde{\gamma}ml)\tilde{\psi}(m, l)$ . Because of the processes of absorption and emission of photons, we write the wave function in the electrodes<sup>23,24</sup>

$$\psi(\mathbf{r}, t) = \sum_n \exp[-i(\epsilon + n\omega)t] \psi_n(\mathbf{r}). \quad (6)$$

Substitution of (6) into (4) gives

$$w^2(\epsilon + n\omega)\psi_n(m, l) = 4\psi_n(m, l) - \exp(i\tilde{\gamma}l)\psi_n(m+1, l) - \exp(-i\tilde{\gamma}l)\psi_n(m-1, l) - \sum_s \Gamma_{ns} \psi_s(m, l-1) - \sum_s \Gamma_{ns}^* \psi_s(m, l+1), \quad (7)$$

where

$$\Gamma_{ns} = i^{s-n} J_{s-n}(\tilde{a}).$$

Here we used the standard expansion of an exponential in Bessel functions<sup>25</sup>

$$\exp(i\tilde{a} \cos \omega t) = \sum_m i^m J_m(\tilde{a}) \exp(im\omega t). \quad (8)$$

Let us introduce column vectors for each site of the square lattice describing the amplitudes of the wave function (6)

$$\Psi(m, l) = \text{col}(\dots, \psi_1(m, l), \psi_0(m, l), \psi_{-1}(m, l), \dots).$$

Then Eq. (7) takes more compact form

$$\begin{aligned} (w^2 \epsilon + \Omega) \Psi &= 4\Psi(m, l) - \exp(i\tilde{\gamma}l) \Psi(m+1, l) \\ &\quad - \exp(-i\tilde{\gamma}l) \Psi(m-1, l) \\ &\quad - \Gamma \Psi(m, l-1) - \Gamma^* \Psi(m, l+1), \end{aligned} \quad (9)$$

where we have introduced two matrices  $\Omega = \text{diag}(w^2 n \omega)$  and  $\Gamma = \{\Gamma_{ns}\}$ . Following Ando<sup>26</sup> we take the electrodes 1 and 4 (Fig. 1c) to be infinitely long in the  $x$  direction and consisting of  $M$  lattice sites in the  $y$  direction. We introduce a generalized vector

$$C_m = \text{col}(\Psi(m, M), \Psi(m, M-1), \dots, \Psi(m, 1)).$$

The dimension of this vector is  $M \times L$  where  $L$  is the dimension of the vector  $\Psi(m, l)$ . In computer simulations the dimension  $L$ , which is the number of amplitudes of the wave function (6), was taken to be a finite number chosen by numerical accuracy.<sup>27</sup> We also introduce a diagonal matrix

$$P_{ll'} = \delta_{ll'} \exp(-i\tilde{\gamma}l),$$

the unit matrices  $I_0$  of dimension  $M \times M$  and  $I$  of dimension  $L \times L$ , and the up-diagonal matrix

$$D = \begin{pmatrix} 0 & 1 & 0 & 0 & \dots \\ 0 & 0 & 1 & 0 & \dots \\ 0 & 0 & 0 & 1 & \dots \\ \vdots & & & & \end{pmatrix}$$

of dimension  $M \times M$ .

Then Eq. (9) takes the form presented by Ando<sup>26</sup>

$$(w^2 \epsilon - H_0) C_m + P_{\parallel} C_{m-1} + P_{\parallel}^* C_{m+1} = 0, \quad (10)$$

where

$$H_0 = 4I_0 \otimes I - D \otimes \Gamma^* - D^+ \otimes \Gamma - I_0 \otimes \Omega, \quad P_{\parallel} = P \otimes I.$$

To obtain the linearly independent modes of Eq. (10) we set<sup>26</sup>

$$C_m = \lambda^m C_0,$$

which gives

$$\lambda \begin{pmatrix} C_1 \\ C_0 \end{pmatrix} = \begin{pmatrix} P_{\parallel}(H_0 - w^2 \epsilon) & -P_{\parallel}^2 \\ 1 & 0 \end{pmatrix} \begin{pmatrix} C_1 \\ C_0 \end{pmatrix}. \quad (11)$$

In order to find similar modes in the perpendicular electrodes (2 and 3 in Fig. 1c) we write the Schrödinger equation (5) as follows:

$$\begin{aligned} (w^2 \epsilon + \Omega) \tilde{\Psi}(m, l) &= 4\tilde{\Psi}(m, l) - \exp(-i\tilde{\gamma}m) \Gamma^* \tilde{\Psi} \\ &\quad \times (m, l+1) - \exp(i\tilde{\gamma}m) \Gamma \tilde{\Psi}(m, l-1) \\ &\quad - \tilde{\Psi}(m+1, l) - \tilde{\Psi}(m-1, l). \end{aligned} \quad (12)$$

Introducing again the column vector  $\tilde{C}_l$  which describes the amplitudes of the  $l$ th line along the  $x$ -direction, we obtain from Eq. (12)

$$(w^2 \epsilon - \tilde{H}_0) \tilde{C}_l + P_{\perp} \tilde{C}_{l-1} + P_{\perp}^* \tilde{C}_{l+1} = 0, \quad (13)$$

where

$$\tilde{H}_0 = 4I_0 \otimes I - D \otimes I - D^+ \otimes I - I_0 \otimes \Omega, \quad P_{\perp} = P^* \otimes \Gamma.$$

Using the relation  $\tilde{C}_l = \lambda^l \tilde{C}_0$  we obtain from (13) the linearly independent solutions in the electrodes 2 and 3:

$$\lambda \begin{pmatrix} \tilde{C}_1 \\ \tilde{C}_0 \end{pmatrix} = \begin{pmatrix} P_{\perp}(\tilde{H}_0 - w^2 \epsilon) & -P_{\perp}^2 \\ 1 & 0 \end{pmatrix} \begin{pmatrix} \tilde{C}_1 \\ \tilde{C}_0 \end{pmatrix}. \quad (14)$$

From the Schrödinger equations (4) and (5) the following continuity equation for the probability density follows:

$$-\frac{w^2}{2} \frac{\partial \rho}{\partial t} = j_{m,l}^{(x)} - j_{m-1,l}^{(x)} + j_{m,l}^{(y)} - j_{m,l-1}^{(y)}, \quad (15)$$

where  $\mathbf{j}_{m,l} = (j_{m,l}^{(x)}, j_{m,l}^{(y)})$  is the probability current density. In particular, for the gauge  $\mathbf{a}_0 = (-\gamma y, 0, 0)$  in the electrodes 1 and 4 we have

$$\begin{aligned} j_{m,l}^{(x)} &= \text{Im}\{\exp(i\tilde{\gamma}l) \psi_{m,l}^* \psi_{m+1,l}\}, \\ j_{m,l}^{(y)} &= \text{Im}\{\exp(-i\tilde{a} \cos \omega t) \psi_{m,l}^* \psi_{m,l+1}\}. \end{aligned} \quad (16)$$

For the gauge  $\mathbf{a}_0 = (0, \gamma x, 0)$  in the electrodes 2 and 3 we have

$$\begin{aligned} j_{m,l}^{(x)} &= \text{Im}\{\tilde{\psi}_{m,l}^* \tilde{\psi}_{m+1,l}\}, \\ j_{m,l}^{(y)} &= \text{Im}\{\exp(-i\tilde{a} \cos \omega t - i\tilde{\gamma}m) \tilde{\psi}_{m,l}^* \tilde{\psi}_{m,l+1}\}. \end{aligned} \quad (17)$$

From these expressions for the probability current density it is easy to find the stationary current carried by the propagating mode with  $|\lambda| = 1$  in the  $x$  direction through the section  $m$  in the electrodes 1 and 4:

$$J_m^{(x)} = \text{Im}(\lambda \langle C_0 | P_{\parallel}^* | C_0 \rangle). \quad (18)$$

As with the mode propagating in the  $y$  direction in the electrodes 2 and 3 we have

$$J_l^{(y)} = \text{Im}(\lambda \langle \tilde{C}_0 | P_{\perp}^* | \tilde{C}_0 \rangle). \quad (19)$$

Now let us consider the scattering region (Fig. 2) connected to four electrodes. Following Ando<sup>26</sup> we define

$$U(\pm) = (\mathbf{u}_1(\pm), \mathbf{u}_2(\pm), \dots, \mathbf{u}_{LM}(\pm)).$$

$$\Lambda(\pm) = \text{diag}(\lambda_1(\pm), \lambda_2(\pm), \dots, \lambda_{LM}(\pm)).$$

Here  $\mathbf{u}_i(\pm)$  are the solutions of Eq. (11) which correspond to the eigenvalue  $\lambda_i(\pm)$ . The signs “ $\pm$ ” refer to the propagating and evanescent modes in the positive (negative)  $x$  direction in the electrodes 1 and 4. Similar matrices  $\tilde{U}, \tilde{\Lambda}$  can be defined for the electrodes 2 and 3.

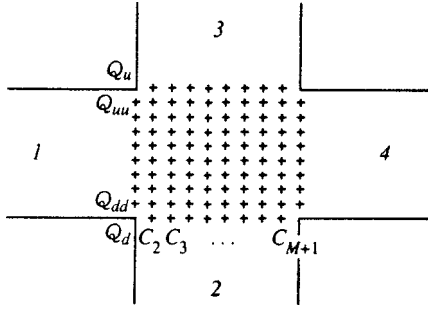


FIG. 2. Configuration of the lattice model for the scattering region.

For the modes which are superpositions only of the “+” type (or of the “-” type) we can write simple recurrence formulas<sup>26</sup>

$$C_{m+1}(\pm) = F(\pm)C_m(\pm)$$

with

$$F(\pm) = U(\pm)\Lambda(\pm)U^{-1}(\pm).$$

The same formulas take place for the electrodes 2 and 3. These relations will be explored to define boundary conditions in the scattering region.

Next, we consider the solutions inside the scattering region which are shown in Fig. 2. At the boundary 1 there is the incident mode  $C_1(+)$ , and at the boundaries 2, 3, and 4 there are only outgoing modes. Introduce vertical vectors  $C_1, C_2, \dots, C_{M+2}$  which describe the amplitudes of the wave function on a square lattice in the scattering region along the  $y$  direction as shown in Fig. 2, and a pair of horizontal vectors  $Q_u, Q_d$  which describe the amplitudes at the upper and down boundaries of the scattering region. The aim is to write closed equations for these vectors using the boundary conditions. The boundary conditions are that the wave is incident only through the left boundary 1 and is given as  $C_1(+)$ , and the other waves exit through all boundaries. Within the scattering region the equation for the amplitudes takes

$$(w^2\epsilon - H_0)C_m + P_{\parallel}C_{m-1} + P_{\parallel}^*C_{m+1} = 0, \quad (20)$$

where  $m = 2, 3, \dots, M + 1$ .

In addition we consider the analogous equations at every boundary. At the boundary 1 we represent the vertical vector  $C_1$  at site 1 as a superposition of the incident and reflected solutions:

$$C_1 = C_1(+) + C_1(-).$$

The vector  $C_0$  belonging to the electrode 1 can be expressed as

$$\begin{aligned} C_0 &= F^{-1}(+)C_1(+) + F^{-1}(-)C_1(-) \\ &= F^{-1}(-)C_1 + (F^{-1}(+) - F^{-1}(-))C_1(+). \end{aligned}$$

Hence the solutions at the right edge of the electrode 1 are expressed in terms of the solutions at sites of the boundary of the scattering region and incident wave. As a result the equation for the amplitudes at the first vertical sites of the scattering region has the form

$$(w^2\epsilon - H_1)C_1 + P_{\parallel}^*C_2 = -P_{\parallel}[F^{-1}(+) - F^{-1}(-)]C_1(+),$$

$$H_1 = H_0 - P_{\parallel}F^{-1}(-).$$

At the boundary 4 we can write similar equations

$$(w^2\epsilon - H_4)C_{M+2} + P_{\parallel}C_{M+1} = 0,$$

$$H_4 = H_0 - P_{\parallel}^*F(+).$$

Since at the boundaries 2 and 3 we have different gauges, we introduce two additional matrices which transform the primary gauge of the wave function:

$$\hat{E}_{u1} = \text{diag}(\exp(i\tilde{\gamma}m(M+1)/2)) \otimes I,$$

$$\hat{E}_{u2} = \text{diag}(\exp(i\tilde{\gamma}m(M-1)/2)) \otimes I.$$

If we take into account these gauge transformations, the equation for the vector  $Q_u$  at the boundary 3 can be written

$$(w^2\epsilon - H_3)E_{u1}Q_u + P_{\perp}E_{u2}Q_{uu} = 0,$$

$$H_3 = \tilde{H}_0 - P_{\perp}^*\tilde{F}(+).$$

At the boundary 2

$$(w^2\epsilon - H_2)E_{u1}^*Q_d + P_{\perp}^*E_{u2}^*Q_{dd} = 0,$$

$$H_2 = \tilde{H}_0 - P_{\perp}\tilde{F}^{-1}(-).$$

Here  $Q_{uu}, Q_{dd}$  denote the horizontal vectors adjacent to the vectors  $Q_u, Q_d$  as shown in Fig. 2.

By means of these relations it is easy to write the Schrödinger equation for the amplitudes at the sites of the scattering region in closed form as  $\hat{K}X = Y$  where  $X = \text{col} \times (C_1, C_2, \dots, C_{M+2}, Q_u, Q_d)$  with the known matrix  $K$  and vector  $Y$ . Numerical solution of this equation gives the solution inside the scattering region, at its boundary, and thereby at each electrode. For the simpler  $L$ - and  $T$ -structures shown in Fig. 1a and 1b the solutions are easily obtained if we set the solutions in the excluded electrodes equal to zero.

In conclusion we comment on the choice of the matrix  $\Gamma$  defined in (7). For an infinite matrix  $\Gamma$  we have the unitary condition  $\Gamma\Gamma^+ = 1$ . If we were to truncate directly the matrix  $\Gamma$  in the numerical calculations the unitary condition would be violated. In turn this would give rise to breakdown of the probability current conservation and what is more crucial, to appearance of undesirable exponentially growing and decaying propagating solutions with small exponents. In order to avoid this difficulty we introduce a new Hermitian matrix  $W$  which determines the matrix  $\Gamma$  as follows

$$\Gamma = \exp(i\tilde{\alpha}W/2), \quad (21)$$

where

$$W = \begin{pmatrix} 0 & 1 & 0 & 0 & \cdots \\ 1 & 0 & 1 & 0 & \cdots \\ 0 & 1 & 0 & 1 & \cdots \\ \vdots & & & & \ddots \end{pmatrix}.$$

Although in the computer simulations the matrix  $W$  is truncated to a finite dimension  $L$ , the relation (21) preserves the unitarity of the matrix  $\Gamma$ .

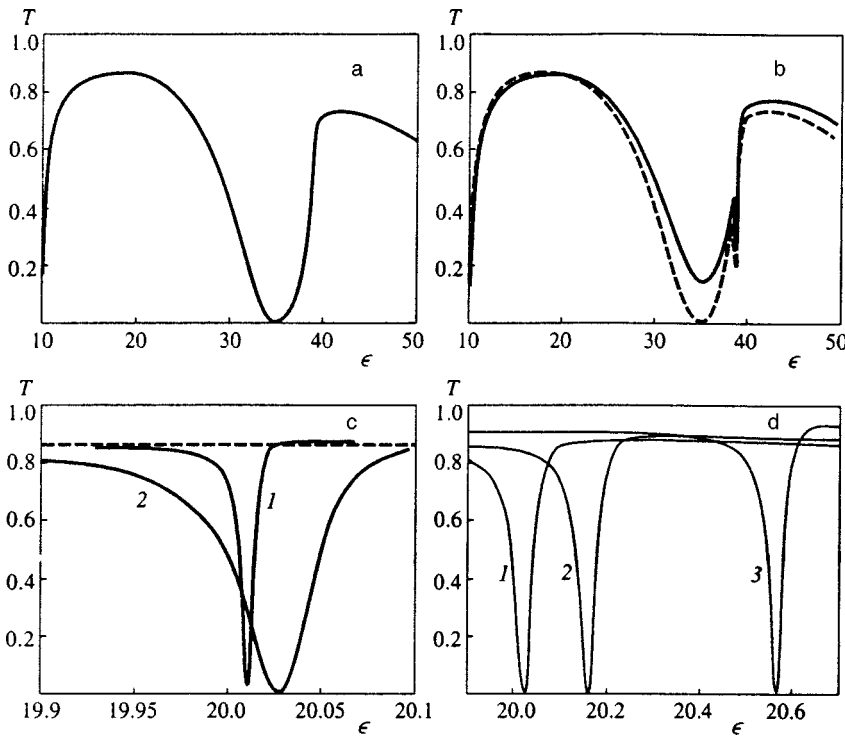


FIG. 3. The energy dependence of the transmission in the  $L$ -structure under the influence of the radiation field: a—stationary transmission  $a=0$  for zero magnetic field; b—the frequency of a radiation field is resonant with transitions between the edges of the first subband and the second one  $\omega=29.6$ ,  $a=0.1$ ,  $\gamma=0$ . The solid line represents the case in which the polarization of the radiation field is perpendicular to the input electrode, the dashed line shows the case, in which the polarization is parallel to the input electrode. c—The frequency of the radiation field is tuned to transitions between the bound state and the first subband  $\omega=10.82$ ,  $\gamma=0$ . The curve 1 corresponds to  $a=0.2$ , the curve 2 to  $a=0.5$ . The dashed line shows the steady case. d—Similar resonant dips with applied magnetic field produced by the radiation field:  $\omega=10.82$ ,  $a=0.5$ . The curves 1, 2, and 3 correspond to  $\gamma=0, 2, 4$  respectively.

## 2.2. Numerical results

We begin by considering the simplest  $L$ -structure (Fig. 1a). It has only one bound state with energy  $\epsilon_0=0.9291\pi^2$ .<sup>14</sup> A magnetic field slightly increases this value. Consider at first the case when the frequency of the radiation field is tuned to transitions between the edges of the second and first subbands,  $\omega\approx 3\pi^2$ . When the polarization  $\mathbf{a}$  of the radiation field is perpendicular to the input electrode of the structure the dipole matrix element mixing states of the second and first subbands equals

$$\langle 1|y|2\rangle = \int dy f_1(y)yf_2(y) \neq 0,$$

where  $f_1(y)=\sqrt{2}\sin(\pi(y-1/2))$ ,  $f_2(y)=\sqrt{2}\sin(2\pi(y-1/2))$ . If the polarization of the radiation field is parallel to the input electrode the dipole matrix element  $\langle k|x|k'\rangle$  calculated in terms of the incident modes  $\exp(ikx)$  is less than  $\langle 1|y|2\rangle$  because of the oscillatory behavior of the functions  $\exp(ikx)$ . Since the square of the dipole matrix element determines the radiation field effect, the electron transmission strongly depends on the polarization of the field as is in fact seen from Fig. 3b.

Second, consider the case when the frequency of the radiation field is resonant with transitions between the bound state energy and the first subband. For zero magnetic field the radiation field induces the deep narrow resonant dip shown in Fig. 3c. The width of the resonant dip depends sensitively on the amplitude of the radiation field. Figure 3d shows the shift of the resonant dip versus the applied magnetic field.

The structure intermediate between the  $L$ - and  $X$ -structure is the  $T$ -structure (Fig. 1b). Like the  $L$ -structure, it has only one bound state provided that the whole structure has the same width, but there are two ways to direct an

incident electron: through the electrode 1 and through the electrode 2. For the former case the transmissions  $T_{12}$  and  $T_{13}$  coincide, provided that  $\gamma=0$ . The polarization of a radiation field is chosen perpendicular to the input electrode along the  $y$ -axis (Fig. 1b). Consider the dipole matrix element between the bound state and the propagating one,  $\langle \chi_1|y|\psi_{k,1}\rangle$ , where  $\chi_1(x,y)$  denotes the bound state with the energy  $\epsilon_1=7.98$  and  $\psi_{k,1}(x,y)$  is the propagating state for the steady case describing an electron incident on the first subband and the electrode 1. Since both states are even relative to inversion  $y\rightarrow -y$  around the symmetry line  $y=0$  (for  $\gamma=0$ ), this dipole matrix element vanishes and the radiation field produces no effect. In fact, our numerical calculations show that if the incident electron propagates in the first subband at zero magnetic field there are no resonant phenomena resulting from the radiation field.

There are two ways to the dipole matrix element can be finite. The first one is to apply an external magnetic field, and the second one is to consider electron transport in the second subband. These possibilities are shown in Fig. 4a and 4b. The steady transmissions through the  $T$ -structure are shown by thin lines. One can see that a magnetic field makes the transmissions  $T_{12}$  and  $T_{13}$  nonequivalent. Application of the radiation field gives rise to resonant dips which are very narrow, with widths proportional to the square of the amplitude of the radiation field. In the vicinity of the resonance the transmission  $T_{13}$  exceeds the transmission  $T_{12}$  which gives rise to the anomalous Hall effect. This effect was first demonstrated for the four-terminal structure.<sup>21</sup>

If an electron is incident on the second electrode, the dipole matrix element is not zero, and we expect resonant behavior for the transmissions to both electrodes 1 and 3. However, the radiation field produces a resonant dip only for the transmission  $T_{23}$  (Fig. 4c). The reason for the absence of

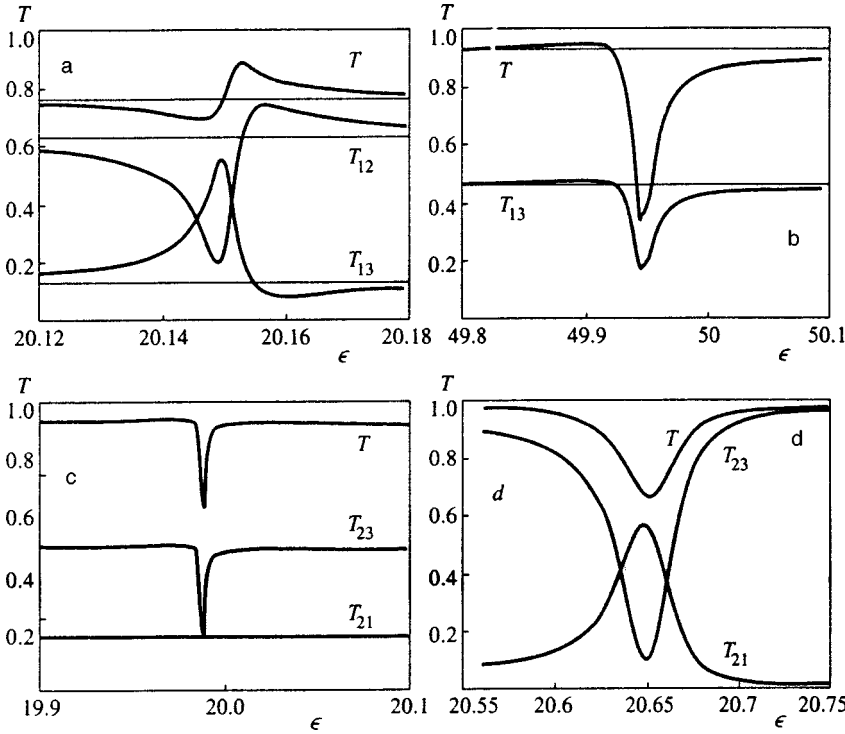


FIG. 4. Transmissions through the  $T$ -structure. a—Electron incidents on the electrode 1 (see Fig. 1b) and the first subband:  $\omega=12$ ,  $a=0.2$ ,  $\gamma=2$ . b—Electron incidents on the second subband with parameters  $\omega=41.86$ ,  $a=0.5$ ,  $\gamma=0$ . c—Electron incidents on the electrode 2,  $\omega=12$ ,  $a=0.1$ ,  $\gamma=0$ . d—The same as in Fig. 4c with parameters  $\omega=12$ ,  $a=0.5$ ,  $\gamma=4$ .

a resonant dip for the transmission to the first electrode is related to the more complicated symmetry and will be given below. Application of an external magnetic field causes the resonant dips for all transmissions shown in Fig. 4d. Also because the bound state energy level is increased by an external magnetic field, the location of the resonant dips is slightly shifted as is seen from Fig. 4c and 4d.

Consider the four-terminal junction (Fig. 1c) which is an element of the Hall structures.<sup>6,7,9,19</sup> First, consider the radiation field effects for zero magnetic field, among which the most interesting is the resonant control of the electron transmissions by rotation of the radiation field polarization. As was mentioned for the  $T$ -structure this effect has a purely symmetric origin. However, the symmetry of the  $X$ -structure is higher than that of the  $T$ -structure. Moreover, the  $X$ -structure has two bound states. The one with the energy  $\epsilon_1=6.55$  below the first subband is symmetrical relative to coordinate inversions  $x \rightarrow -x$  or  $y \rightarrow -y$ , and the second with the energy  $\epsilon_2=36.72$  below the second subband is antisymmetric.

As was observed for the  $T$ -structure, if the polarization of the radiation field is perpendicular to the input electrode and the frequency of the field is tuned to the transition between the first subband and the energy of the first symmetrical bound state, there are no field-induced resonant effects in the transmissions. The reason is that the propagating state is even,  $\psi_{k,1}(x,y)=\psi_{k,1}(x,-y)$ , and so we have  $\langle \chi_1 | y | \psi_{k,1} \rangle = 0$ , which means that the transmissions exhibit no resonant effect. On the other hand, there is no symmetry of the propagating state relative to  $x \rightarrow -x$  due to electrons incident on the first electrode along the  $x$ -axis. Therefore, for the case of the polarization parallel to the input electrode 1 the dipole matrix element satisfies  $\langle \chi_1 | x | \psi_{k,1} \rangle \neq 0$ . In fact, one can see from Fig. 5a a narrow resonant peak in the transmission  $T_{14}$ .

However, as in the case of the  $T$ -structure, surprisingly, there are no resonant effects for the transmissions to the electrodes 2 and 3.

To understand this following<sup>21</sup> we perform the gauge transformation

$$\psi(\mathbf{r}, t) = \exp(i\mathbf{a}\mathbf{r} \cos \omega t) \phi(\mathbf{r}, t),$$

and substitute it into Eq. (3). As a result we obtain the following equation for the amplitudes  $\phi_n(\mathbf{r})$  of expansion (6):

$$(\epsilon + n\omega)\phi_n = (i\nabla + \mathbf{a}_0(\mathbf{r}))^2 \phi_n + \frac{i\omega}{2}(\mathbf{a}\mathbf{r})(\phi_{n+1} - \phi_{n-1}). \quad (22)$$

Since we have assumed that the radiation field is resonant with transitions between the first bound state and the propagating one, for small perturbations we can restrict ourselves to two states  $\phi_0$  and  $\phi_{-1}$  in Eq. (22) satisfying the following equations:

$$\nabla^2 \phi_0 + \epsilon \phi_0 = -\frac{i}{2}(\mathbf{a}\mathbf{r})\omega \phi_{-1}, \quad (23)$$

$$\nabla^2 \phi_{-1} + (\epsilon - \omega)\phi_{-1} = \frac{i}{2}(\mathbf{a}\mathbf{r})\omega \phi_0, \quad (24)$$

where the functions  $\phi_0(\mathbf{r})$  and  $\phi_{-1}(\mathbf{r})$  correspond to the propagating and the bound states, respectively. For the resonant case  $\epsilon - \omega \approx \epsilon_1$  we can write the truncated Green's function for the left side of Eq. (24)

$$G_1(\mathbf{r}, \mathbf{r}', \epsilon) \approx \frac{\chi_1(\mathbf{r})\chi_1^*(\mathbf{r}')}{\epsilon - \epsilon_1 - i\delta} \quad (25)$$

where  $\delta$  accounts for the finite width of the level because of coupling of the structure with the electrodes and the mixing

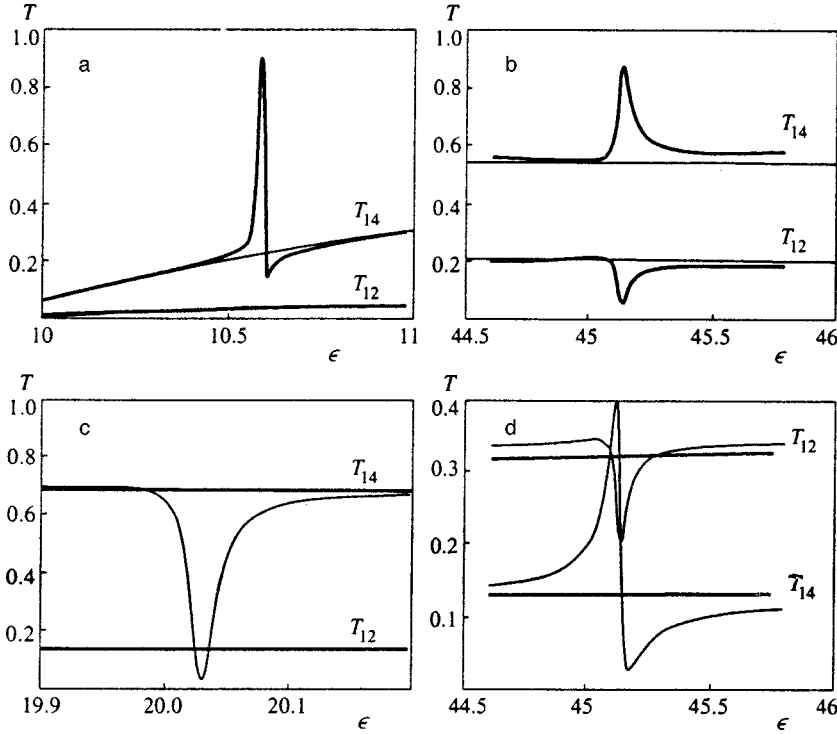


FIG. 5. Transmissions through the X-structure for zero magnetic field. In all pictures the electron is incident on the electrode 1. a—The frequency of the radiation field is tuned to transitions between the energy of the first bound state and bottom of the first subband,  $\omega=4$ . The case of the polarization of the radiation field along the input electrode is shown by thick lines, and the case of the polarization perpendicular to the input electrode is shown by thin lines. In both cases the amplitude of the radiation field is  $a=0.05$ . The electron is incident on the first subband ( $n=1$ ). b— $\omega=38.45$ ,  $a=0.5$ , the electron is incident on the first subband. c—The frequency is tuned to transitions between the second bound state and the first subband.  $\omega=16.715$ ,  $a=0.2$ . d—As in Fig. 5b, but the electron is incident on the second subband ( $n=2$ ).

of propagating states with the bound state by the radiation field. Then a solution of Eq. (24) can be expressed via the Green's function (25) as follows:

$$\phi_{-1}(\mathbf{r}) = \frac{i\omega\chi_1(\mathbf{r})}{2(\epsilon - \omega - \epsilon_1 - i\delta)} \times \int \chi_1^*(\mathbf{r}')(\mathbf{a}\mathbf{r}')\phi_{0h}(\mathbf{r}')d^2\mathbf{r}'. \quad (26)$$

Substituting Eq. (23) and carrying out a similar procedure of expression in terms of the Green's function, we finally obtain

$$\phi_0(\mathbf{r}) = \phi_{0h}(\mathbf{r}) + \frac{\omega^2 d_{10}}{4(\epsilon - \epsilon_1 - \omega - i\delta)} \times \int G(\mathbf{r}, \mathbf{r}', \epsilon)(\mathbf{a}\mathbf{r}')\chi_1(\mathbf{r}')d^2\mathbf{r}'. \quad (27)$$

Here  $\phi_{0h}(\mathbf{r})$  is the solution for a switched off radiation field and

$$d_{10} = \int \chi_1^*(\mathbf{r})(\mathbf{a}\mathbf{r})\phi_{0h}(\mathbf{r})d^2\mathbf{r}$$

is the dipole matrix element between the bound state and the propagating one.

Similar to (26) and (27) we can write a solution of Eq. (24) for the case when the frequency of the radiation field is resonant with transitions between the second bound state and the Fermi energy of the incident electron  $\epsilon + \omega \approx \epsilon_2$

$$\phi_0(\mathbf{r}) = \phi_{0h}(\mathbf{r}) + \frac{\omega^2 d_{20}}{4(\epsilon - \epsilon_2 + \omega - i\delta)} \times \int G(\mathbf{r}, \mathbf{r}', \epsilon)(\mathbf{a}\mathbf{r}')\chi_2(\mathbf{r}')d^2\mathbf{r}',$$

$$d_{20} = \int \chi_2^*(\mathbf{r})(\mathbf{a}\mathbf{r})\phi_{0h}(\mathbf{r})d^2\mathbf{r} \quad (28)$$

In order to analyze the transmission on the basis of Eq. (27) we need the following symmetry properties of the Green's function in the X-structure:

$$G(x, y; x', y', \epsilon) = G(-x, y; -x', y', \epsilon) \\ = G(x, -y; x', -y', \epsilon). \quad (29)$$

Now let us return to the transmission  $T_{12}$  (Fig. 1c) for the case when the radiation field polarization is parallel to the input electrode ( $x$ -axis). From Eqs. (27) and (29) we can see that the last resonant term in (27) is odd relative to  $x \rightarrow -x$  in the electrodes 2 and 3, provided that the bound state  $\chi_1(\mathbf{r})$  is even. Thus, the last term in (27) is not able to contribute to the propagating mode in the electrodes 2 and 3 because for the electron transport in the first subband it should be even with respect  $x \rightarrow -x$ . Next, since the last term in (27) is even with respect  $y \rightarrow -y$ , it contributes to the even transport mode  $\phi_0$  in the electrodes 1 and 4. As we see from Fig. 5a computer calculations completely confirm that conclusion. If the incident electron belongs to the first subband with  $n=1$  (even state relative to  $y \rightarrow -y$ ), but the outgoing mode can be represent as a superposition of states of the first and second subband ( $n=1,2$ ), these symmetry restrictions are removed for the polarization parallel to the input electrode. As a result the radiation field induces resonant anomalies in the transmissions  $T_{12}$ ,  $T_{13}$  (see Fig. 5b). Briefly, this symmetry rule can be formulated as follows. If the parity of the state excited by the dipole transition  $(\mathbf{a}\mathbf{r})\chi_1(\mathbf{r})$  does not conflict with the parity of the outgoing modes, then the transmission to the corresponding electrode can display resonant features,

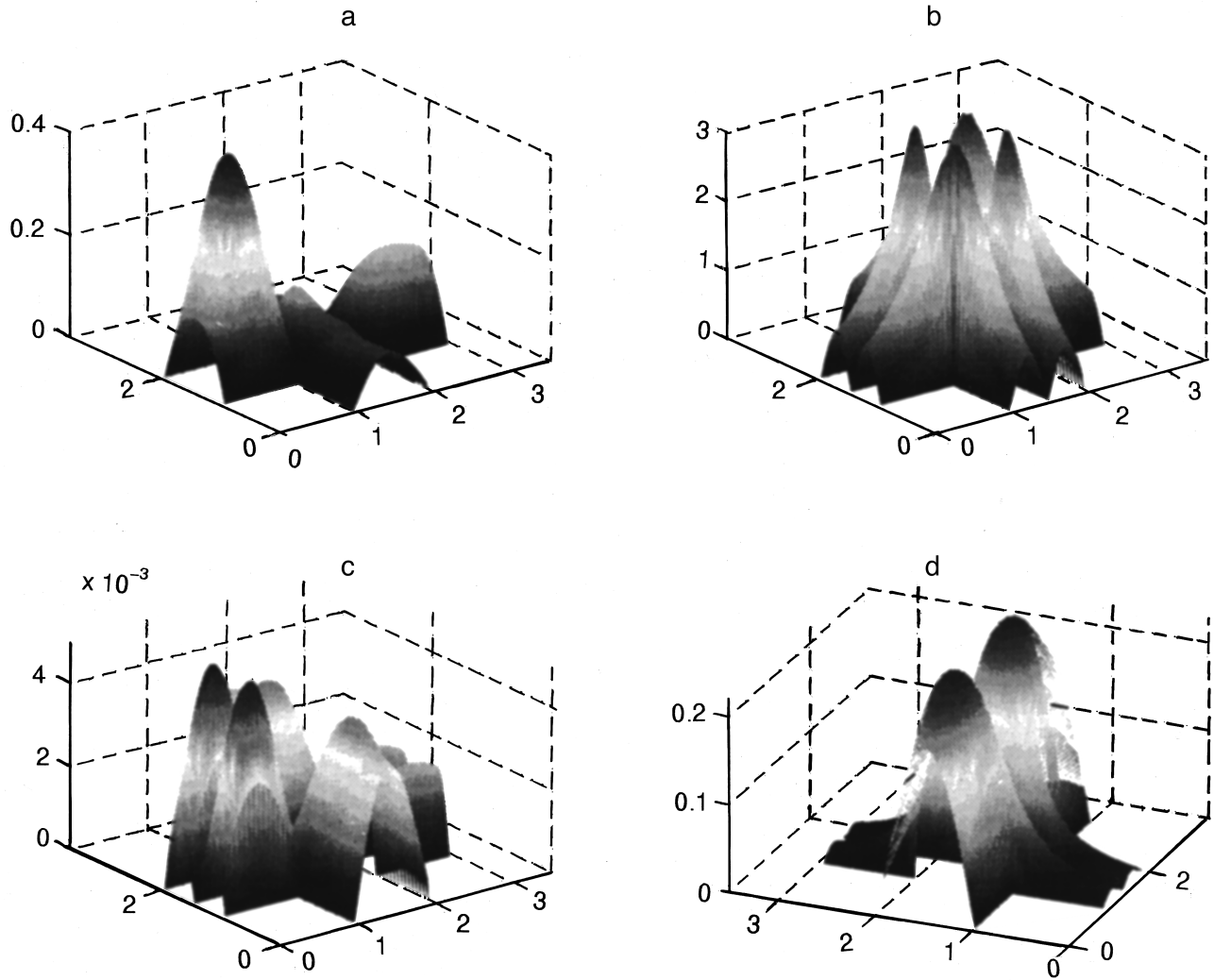


FIG. 6. Views of the amplitudes of the quasienergy wave function  $\epsilon=20.02$ ,  $a=0.2$ ,  $\omega=16.715$ . a— $|\psi_0(\mathbf{r})|$ , b— $|\psi_1(\mathbf{r})|$ , c— $|\psi_{-1}(\mathbf{r})|$ , d— $|\psi_0(\mathbf{r}) - \psi_{0h}(\mathbf{r})|$ . Definitions of the amplitudes are given in (6).

and vice versa. Later we will demonstrate numerous examples of the application of this symmetry rule.

First, we apply the symmetry rule to the case of radiation field mixing of the second bound state, which is odd relative to  $x \rightarrow -x$  or  $y \rightarrow -y$ . For the radiation field polarization directed parallel to the input electrode the dipole matrix element  $d_{20}$  vanishes, and consequently there are no radiation field induced effects. In the opposite case, when the polarization is perpendicular to the input electrode, the dipole matrix element is not equal to zero. However, the radiation field contribution to the electrodes 2 and 3 described by the last term in Eq. (26) is odd, opposite to the symmetry of the incident mode. So the transmissions to the electrodes 2 and 3 coincide with steady results, as shown in Fig. 5c. Finally, Fig. 5d shows the case when the incident electron belongs to the second subband. In contrast to the case in Fig. 5b, the field-induced effects take place when the polarization is perpendicular to the input electrode. Note that the same symmetry arguments explain the absence of radiation field effects in the electron transmission from electrode 2 to electrode 1 shown in Fig. 4c for the  $T$ -structure.

To confirm the approach using the quasi energy ampli-

tudes (26) and (27) and to illustrate symmetry rules, in Fig. 6 we present numerical solutions of the full Schrödinger equation (4). In Fig. 6a, 6b, and 6c the amplitudes  $\psi_n(\mathbf{r})$  with  $n=0,1,-1$  respectively are shown for parameters corresponding to the case shown in Fig. 5c. One can see that, in fact, only two amplitudes,  $\psi_0$ ,  $\psi_1$ , are important in the resonant case. Moreover, in agreement with Eq. (28) we see that the amplitude  $\psi_1(\mathbf{r})$  exactly reproduces the second bound wave function  $\chi_2$  and that the next amplitude  $\psi_{-1}$  is negligible. Second, the difference between the radiation field perturbed solution  $\psi_0$  and the steady solution  $\psi_{0h}$  is shown in Fig. 6d. One can see that symmetry of the outgoing part of this difference in the electrodes coincides with that predicted by the last term in Eq. (28). The parity is even in the electrodes 1 and 4 and is odd in the electrodes 2 and 3. Also we can see from Fig. 6d that the odd contributions are decaying in the electrodes 1 and 3.

As was mentioned above an external magnetic field breaks the symmetry of the structure, resulting in a more complicated picture of radiation field effects. Results of these calculations are presented in Fig. 7. Figure 7a corresponds to Fig. 5a, with the difference that we have  $\gamma=1$ , and presents

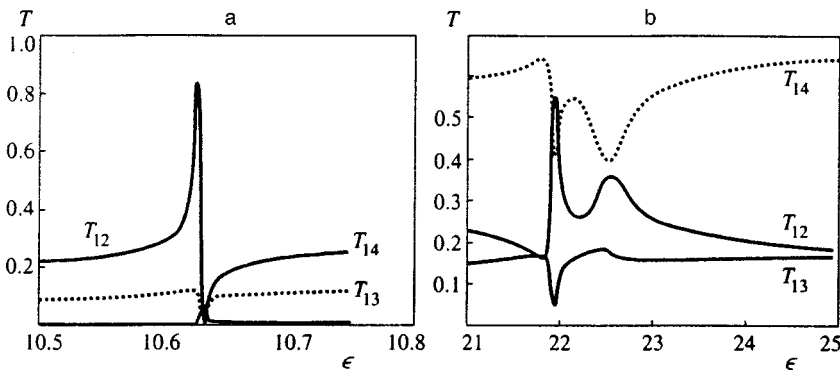


FIG. 7. The energy dependences of the transmissions in applied magnetic field in the X-structure. a— $\omega=4$ ,  $a=0.05$ ,  $\gamma=1.0$ , the polarization of the radiation field is parallel to the input electrode; b— $\omega=15.08$ ,  $a=0.5$ ,  $\gamma=2$ , polarization of the radiation field is perpendicular to the input electrode.

a case in which the radiation field excites the first bound state in the first subband. One can see all transmissions undergo resonant peaks or dips, in contrast to Fig. 5a. Figure 7b presents a case in which the frequency of the radiation field is tuned to  $\omega=(\epsilon_2-\epsilon_1)/2$ . One can see that exciting of two bound states results in two resonant peaks in the transmissions. The first bound state gives rise to sharp resonant peaks and dips, while the second produces wide peaks and dips.

From Fig. 7b we can see that in some narrow region of energies the transmission  $T_{13}$  coincides with  $T_{12}$  and may even slightly exceed it. Obviously, it would give rise to the negative Hall resistance as was shown in Ref. 21. Moreover we can see from Fig. 7b that the transmission  $T_{12}$  undergoes peaks, while the transmission  $T_{13}$  does dips. As a result we may observe resonant peaks in the Hall resistance as is demonstrated in Fig. 8.

From Fig. 7a and 7b (see also Ref. 21) in the narrow region of resonance the transmission  $T_{13}$  can slightly exceed the transmission  $T_{12}$  in an external magnetic field. This means that the radiation field can even cause anomalies of the Hall resistance to be negative.<sup>21</sup> Figure 8 illustrates vari-

ous resonant anomalies of the Hall resistance induced by the radiation field: dips (Fig. 8a) and peaks (Fig. 8b, 8c, and 8d). The resonance between the first bound state and the Fermi energy of the incident electron produces a resonant dip (Fig. 8a). In the case of the Fermi energy  $\epsilon \approx (\epsilon_2 + \epsilon_1)/2$  and  $\omega \approx (\epsilon_2 - \epsilon_1)/2$  the radiation field induces two wide peaks contributed by two bound states. Figure 8c shows that the radiation field transforms the dip in the Hall resistance<sup>6</sup> into a resonant peak. Finally, Fig. 8d shows a case like Fig. 8a, but the radiation field excites the second bound state.

3. CONCLUSION

The resonant behavior in the electron transmission arises because the radiation field resonantly substitutes the bound states into the state of the incident electron propagating through the scattering region of the structures to produce various interference phenomena. These phenomena are clearly seen in the current density patterns shown in Fig. 9. The resonant anomalies are very specific to the forms the structure and the type of bound state. The symmetry of the

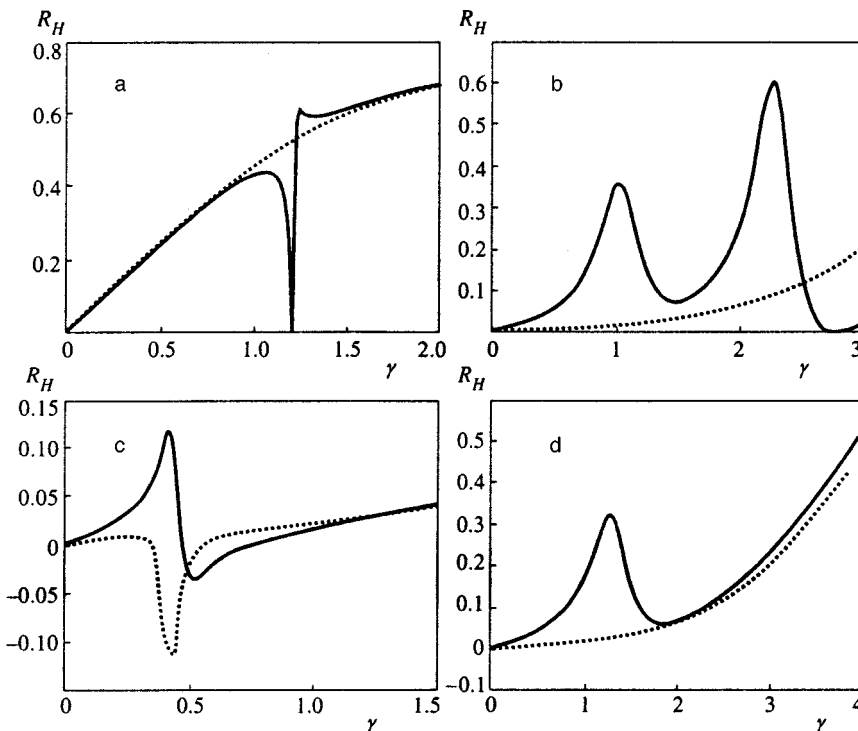


FIG. 8. The Hall resistance  $R_H$  in the X-structure versus an external magnetic field in response to the radiation field. The radiation field induced resistance is shown by solid lines, the steady resistance is shown by dotted line. a— $\epsilon=10.95$ ,  $\omega=4.3$ ,  $a=0.05$ ; b— $\epsilon=22$ ,  $\omega=15.08$ ,  $a=0.5$ ; c— $\epsilon=36.75$ ,  $\omega=30.17$ ,  $a=0.1$ ; d— $\epsilon=20.5$ ,  $\omega=16.715$ ,  $a=0.5$ .

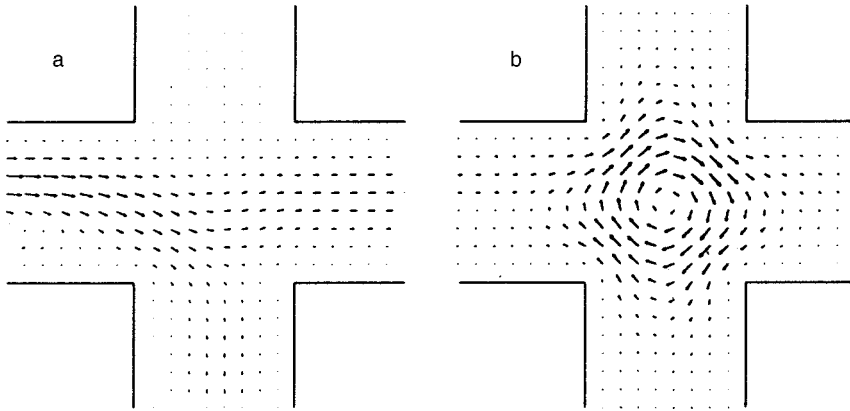


FIG. 9. Current density flowing in the X-structure when the radiation field is switched off (a) and switched on (b);  $\omega=4.3$ ,  $a=0.05$ ,  $\epsilon=10.95$ ,  $\gamma=1.21$ .

structure and corresponding parity of the bound state plays an important role for the radiation field-induced effects because of symmetry rules for the dipole matrix element and for the resonant contribution, which is described by the right side of Eqs. (27) and (28). As a result the direction of the radiation field's polarization relative to the input electrode has strong effect on the resonant anomalies. This suggests an idea for controlling electron transmissions through the corresponding electrodes by simple rotation of the polarization of the radiation field.

In conclusion we give dimensional estimates for the radiation field which is able to produce resonant effects in the 2DEG. The Fermi energy in the semiconductor layered AlGaAs structures depends on the density of the electron gas and typically lies between 10 meV and 100 meV. The characteristic sizes  $d$  of the structures are between 100 nm and 1  $\mu\text{m}$ . Accordingly, the frequency of the radiation field tuned to transitions between the bound states and the first electron subband will be roughly proportional to the Fermi energy. The amplitude of the radiation field is of order  $E \approx E_F a \omega / ed \sim 10^3 - 10^4$  V/cm, where  $a$  and  $\omega$  are dimensionless.

A. F. S. thanks K.-F. Berggren, P. Šeba and S. Wang for useful discussions of electron transport in waveguides. This work was partially supported by the INTAS-RFBR (Grant No. 95-IN-RU-657), RFFI (Grant No. 97-02-16305), Krasnoyarsk Science Foundation (Grant No. 7F0130) and the Foundation for Theoretical Physics in Slemeno, Czech Republic.

\*E-mail: zeos@zeos.krascience.rssi.ru

<sup>1</sup>B. J. van Wees, H. van Houten, C. W. J. Beenakker, J. G. Williamson, L. P. Kouwenhouen, D. van der Marel, and C. T. Foxon, Phys. Rev. **60**, 848 (1988).

- <sup>2</sup>D. A. Wrahamn, T. J. Thornton, R. Newbury, M. Pepper, H. Ajmed, J. E. F. Frost, D. G. Hasko, D. C. Peacock, D. A. Ritchie, and G. A. C. Jones, J. Phys. C **21**, L209 (1988).
- <sup>3</sup>M. L. Roukes, A. Sherer, S. J. Allen, Jr., H. G. Craighead, R. M. Ruthen, E. D. Beeke, and J. P. Harbison, Phys. Rev. Lett. **59**, 3011 (1987).
- <sup>4</sup>Y. Takagaki, K. Gamo, S. Namba, S. Ishida, S. Takaoka, K. Murase, K. Ishibashi, and Y. Aoyagi, Solid State Commun. **68**, 1051 (1988).
- <sup>5</sup>C. J. B. Ford, S. Washburn, M. Büttiker, C. M. Knoedler, and J. M. Hong, Phys. Rev. Lett. **62**, 2724 (1989).
- <sup>6</sup>R. L. Schult, D. G. Ravenhall, and H. W. Wyld, Phys. Rev. B **41**, 12760 (1990).
- <sup>7</sup>K. Amemiya and K. Kawamura, J. Phys. Soc. Jpn. **63**, 3087 (1994).
- <sup>8</sup>R. L. Schult, D. G. Ravenhall, and H. W. Wyld, Phys. Rev. B **39**, 5476 (1989).
- <sup>9</sup>F. M. Pecters, Superlattices Microstruct. **6**, 217 (1989).
- <sup>10</sup>H. Sakaki, in *Proc. of the Intern. Symp. on Foundation of Quantum Mechanics in the Light of New Technology*, ed. by S. Kameluchi, Physical Society of Japan, Tokyo (1984), p. 94.
- <sup>11</sup>J. P. Carini, J. T. Londergan, K. Mullen, and D. P. Murdock, Phys. Rev. B **46**, 15538 (1992).
- <sup>12</sup>J. P. Carini, J. T. Londergan, K. Mullen, and D. P. Murdock, Phys. Rev. B **48**, 4503 (1993).
- <sup>13</sup>P. Exner and P. Šeba, J. Math. Phys. **30**, 2574 (1989).
- <sup>14</sup>P. Exner, P. Šeba, and P. Štoviček, Czech. J. Phys., Sect. B **39**, 1181 (1989).
- <sup>15</sup>Y. Avishai, D. Bessis, B. G. Giraud, and G. Mantica, Phys. Rev. B **44**, 8028 (1991).
- <sup>16</sup>J. Goldstone and R. L. Jaffe, Phys. Rev. B **45**, 14100 (1992).
- <sup>17</sup>P. Duclos and P. Exner, Rev. Math. Phys. **7**, 73 (1995).
- <sup>18</sup>K. Lin and R. L. Jaffe, E-prints archive cond-mat/9601004.
- <sup>19</sup>Y. Avishai, and Y. B. Band, Phys. Rev. Lett. **62**, 2527 (1989).
- <sup>20</sup>K.-F. Berggren and Z.-L. Ji, Phys. Rev. **43**, 4760 (1991).
- <sup>21</sup>E. N. Bulgakov and A. F. Sadreev, JETP Lett. **66**, 431 (1997).
- <sup>22</sup>R. E. Peierls, Z. Phys. **80**, 763 (1933).
- <sup>23</sup>M. Büttiker and R. Landauer, Phys. Rev. Lett. **49**, 1739 (1982).
- <sup>24</sup>D. L. Haavig and R. Reifenberger, Phys. Rev. B **26**, 6408 (1982).
- <sup>25</sup>*Handbook of Mathematical Functions*, ed. by M. Abramowitz and I. A. Stegun, U.S. GPO, Washington, DC (1964).
- <sup>26</sup>T. Ando, Phys. Rev. B **44**, 8017 (1991).
- <sup>27</sup>E. N. Bulgakov and A. F. Sadreev, J. Phys.: Condens. Matter **8**, 8869 (1996).

Published in English in the original Russian journal. Reproduced here with stylistic changes by the Translation Editor.